THE JOURNAL OF PHYSICAL CHEMISTRY B

Article

Cite This: J. Phys. Chem. B 2019, 123, 7885−7892

pubs.acs.org/JPCB

Reliability of Poisson−Nernst−Planck Anomalous Models for Impedance Spectroscopy

E. K. Lenzi,[†] L. R. Evangelista,[‡,△] L. Taghizadeh,[§] D. Pasterk,[§] R. S. Zola,[*,∥] T. Sandev,[⊥,#] C. Heitzinger,[§] and I. Petreska[#]

[†]Departamento de Física, Universidade Estadual de Ponta Grossa, Avenida Av. General Carlos Cavalcanti 4748, 84030-900 Ponta Grossa, Paraná, Brazil

[‡]Departamento de Física, Universidade Estadual de Maringá, Avenida Colombo 5790, 87020-900 Maringá, Paraná, Brazil

[§]Institute for Analysis and Scientific Computing, Vienna University of Technology (TU Wien), Wiedner Hauptstraße 8−10, 1040 Vienna, Austria

[∥]Departamento de Física, Universidade Tecnológica Federal do Paraná—Apucarana, PR 86812-460, Brazil

[⊥]Research Center for Computer Science and Information Technologies, Macedonian Academy of Sciences and Arts, Bul. Krste Misirkov 2, 1000 Skopje, Macedonia

[#]Institute of Physics, Faculty of Natural Sciences and Mathematics, Ss. Cyril and Methodius University, Arhimedova 3, 1000 Skopje, Macedonia

ABSTRACT: We investigate possible connections between two different implementations of the Poisson−Nernst−Planck (PNP) anomalous models used to analyze the electrical response of electrolytic cells. One of them is built in the framework of the fractional calculus and considers integro-differential boundary conditions also formulated by using fractional derivatives; the other one is an extension of the standard PNP model presented by Barsoukov and Macdonald, which can also be related to equivalent circuits containing constant phase elements (CPEs). Both extensions may be related to an anomalous diffusion with subdiffusive characteristics through the electrical conductivity and are able to describe the experimental data presented here. Furthermore, we apply the Bayesian inversion method to extract the parameter of interest in the analytical formulas of impedance. To resolve the corresponding inverse problem, we use the delayed-rejection adaptive-Metropolis algorithm (DRAM) in the context of Markov-chain Monte Carlo (MCMC) algorithms to find the posterior distributions of the parameter and the corresponding confidence intervals.

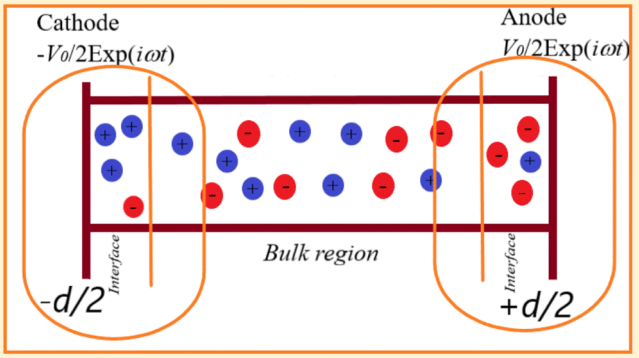

INTRODUCTION

The impedance response of electrolytic cells gives a variety of information, enabling comprehension of the complex diffusion phenomena in liquid/solid interfaces, that are of crucial importance for a vast number of technological applications, as well as for life-sustaining processes. In this context, the AC small-signal immittance (impedance or admittance) spectroscopy (IS) represents a powerful method for characterization of many electrical properties of materials and can be used to investigate the dynamics of bound or mobile charge in the bulk or interfacial regions.[1,2] In addition, the electrical quantities obtained by IS may also be related to physical parameters of these systems, which are directly connected with the ion motion. The models frequently used to analyze the data are essentially based on diffusion-like equations for the ions, satisfying the Poisson's equation requirement for the electric potential (this is the so-called Poisson−Nernst−Planck or PNP model), or on equivalent circuits.[1] In the context of the diffusion equations, typical approaches use boundary conditions such as perfect blocking electrodes,[3] Chang−Jaffé processes,[4] and adsorption−desorption processes,[3] among others, to model the surface effects. However, these situations can be worked out in a unified way, as particular cases, by considering integral-differential boundary conditions as the ones discussed in ref 5 and references therein. Such boundary conditions aim at incorporating behaviors that may not be well-described in terms of the standard formulation of the diffusive PNP model, as is the emblematic case of anomalous diffusion. On the other hand, an important extension used in the framework of equivalent circuits is the introduction of a constant phase element (CPE), whose presence can be connected to the necessity to describe unusual effects in

Received: July 1, 2019
Revised: August 6, 2019
Published: August 12, 2019

DOI: 10.1021/acs.jpcb.9b06263
J. Phys. Chem. B 2019, 123, 7885−7892

many solid electrode/electrolyte interfaces. For instance, Jorcin et al.[6] have pointed out that simple elements alone cannot describe frequency dispersion often found in a solid electrode/electrolyte interface, mainly in the low-frequency domain.

In this paper, we analyze the possible connections between two different extensions of the PNP model for impedance spectroscopy including anomalous diffusive behavior, which have recently been proposed. We also focus on their relations with equivalent circuits (mainly the ones involving CPEs) and anomalous diffusion processes. One of the models was formulated and applied in refs 7−11, being based on integro-differential boundary conditions to be satisfied by the solutions of the diffusion equations (usual and fractional). The other extension was presented in refs 1, 2, and 12 and is also aimed at extending the usual PNP model. These extensions have proved to be powerful tools to reproduce the experimental behavior of the impedance, $\mathcal{Z} \sim 1/(i\omega)^{\delta}$ $(0 < \delta < 1)$, in the low-frequency limit. A peculiar behavior in this limit is found in several different contexts, including liquid-crystalline samples,[13] fractal electrodes,[14] nanostructured iridium oxides,[15] water systems,[16] morphology and ion conductivity of gelatin−$LiClO_4$ films,[17] and weak electrolytic solutions,[1] among many others. In all these systems, the impedance spectroscopy response exhibits very rich and complex behaviors, thus requiring more sophisticated theoretical models to interpret them properly. In the present paper, we test both of the considered models by comparison to the experimental data for Milli-Q water, which is a reference for various investigations of ultrapure water and water systems, applying Bayesian inversion to extract the model parameters.

TWO PNPA MODELS AND THEIR CONNECTIONS

Let us recall the extension of the PNP model that takes into account general boundary conditions expressed in terms of an integro-differential equation, along the lines discussed in more details in refs 18 and 19. This model considers for the bulk densities of ions n_α ($\alpha = +$ for positive and $\alpha = -$ for negative ones) the dynamics given in terms of the standard diffusion equation. It can be obtained from the continuity equations

$$\frac{\partial}{\partial t} n_\alpha(z, t) = -\frac{\partial}{\partial z} \mathcal{J}_\alpha(z, t) \tag{1}$$

with the drift-diffusion current density given by

$$\mathcal{J}_\alpha(z, t) = -D_\alpha \frac{\partial}{\partial z} n_\alpha(z, t) \mp \frac{qD_\alpha}{k_B T} n_\alpha(z, t) \frac{\partial V(z, t)}{\partial z} \tag{2}$$

where, for simplicity, it will be assumed that $D_+ = D_- = D$; i.e., the diffusion coefficients for positive and negative ions are alike. The quantities k_B and T are the Boltzmann constant and the absolute temperature, respectively. $V(z, t)$ is the effective electric potential across a typical sample of thickness d, with the electrodes placed at the positions $z = \pm d/2$. The potential, in the drift term of eq 2, must satisfy Poisson's equation

$$\frac{\partial^2}{\partial z^2} V(z, t) = -\frac{q}{\varepsilon}[n_+(z, t) - n_-(z, t)] \tag{3}$$

in which ε is the dielectric constant of the medium (measured in ε_0 units). The solutions for $n_-(z, t)$ and $n_+(z, t)$, obtained from the equations which emerge after substituting eqs 1 in 2, have to satisfy the boundary condition

$$\mathcal{J}_\alpha\left(\pm\frac{d}{2}, t\right) = \pm \int_{-\infty}^{t} dt' \int_0^1 d\nu \kappa_\alpha(t - t', \nu) \frac{\partial^\nu}{\partial t'^\nu} n_\alpha\left(\pm\frac{d}{2}, t'\right) \tag{4}$$

In eq 4, the kernel, convoluted with the fractional derivative (of order ν, with $0 < \nu \leq 1$) of the bulk density of charges calculated at the surfaces, may be chosen to describe, as particular cases, many other physical situations (as previously discussed) and considered elsewhere (see, e.g., refs 18, 20−22). One of them is the case characterized by perfectly blocking electrodes, which corresponds to $\kappa_\alpha(t, \nu) = 0$ and leads to an accumulation of charges on the surface of the electrode. For $\kappa_\alpha(t, \nu) = \kappa e^{-t/\tau}\delta(\nu - 1)$, which implies $\overline{\kappa}_\alpha(i\omega) = \kappa\tau/(1 + i\omega\tau)$, we have a standard situation characterized by sorption−desorption processes, in which the parameter κ is related to the sorption process and τ is related to the desorption process. A similar case was essentially worked out in refs 3, 5, and 21 by considering the processes on the surface of the electrode governed by a kinetic equation of first order. In the low-frequency limit, these cases lead to $\mathcal{Z} \sim 1/(i\omega)$, which is different from the behavior $\mathcal{Z} \sim 1/(i\omega)^{\delta}$ exhibited in many experimental situations as mentioned before. Such scenarios may be attributed to unusual relaxation processes related to non-Debye relaxations, which may be handled in terms of a fractional kinetic equation. Furthermore, the asymptotic result for the impedance is related with the behavior exhibited by CPEs, which in turn may be related to differential operators of fractional order.[5,23] Thus, in order to cover a broad set of relevant experimental situations, we unify and extend, from the formal point of view, the previous boundary conditions to a fractional one with the possibility of describing a wide range of scenarios depending on the choice of the kernel $\kappa(t, \nu)$ and the fractional differential operator. This extended approach is able to reproduce the behavior $\mathcal{Z} \sim 1/(i\omega)^{\delta}$ exhibited by the experimental data and permits one to consider the superposition of different surface phenomena according to the choice of the kernel. The effective electrical potential coming from eq 3 has to satisfy the condition $V(\pm d/2, t) = \pm (V_0/2)e^{i\omega t}$ on the electrode surfaces, where ω is the frequency of the applied potential and V_0 its amplitude, Figure 1.

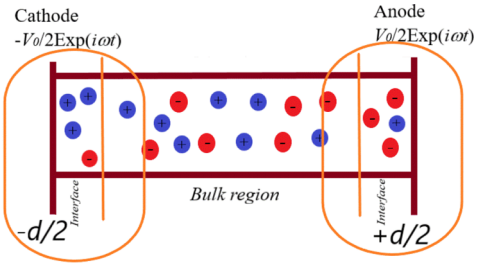

Figure 1. Sketch of the electrolytic cell showing the effective thickness of the sample between the two electrode surfaces.

The set formed from eqs 1−4 represents the mathematical statement of a very general PNPA (where "A" stands for "anomalous") diffusive model based on constitutive equations. To obtain analytic solutions for this problem is always a formidable task. However, for the investigation of electrical impedance, one usually assumes that the applied periodic potential has a very small amplitude, which corresponds to the AC small-signal limit. Thus, an exact solution and, con-

DOI: 10.1021/acs.jpcb.9b06263
J. Phys. Chem. B 2019, 123, 7885−7892

sequently, an analytic expression for the electrical impedance (or admittance) can be determined. The details of the calculation can be found elsewhere,[18] but it is necessary to underline here that, in this limit, one can assume $n_\alpha(z, t) = N + \eta(z)e^{i\omega t}$ with $N \gg |\eta(z)e^{i\omega t}|$, where N represents the number of ions per unit volume. This allows one to assume also that $V(z, t) = \phi(z)e^{i\omega t}$ analyzes the impedance, since the stationary state is reached. After performing some calculations, one is able to show that the impedance is[18]

$$\mathcal{Z}_{\mathrm{PNPA},1} = \frac{2}{i\omega S\epsilon\beta^2}\frac{\tanh(\beta d/2)/(\lambda_D^2\beta) + (d/2\mathcal{D})\mathcal{E}(i\omega)}{1 + \bar{\kappa}_\alpha(i\omega)(1 + i\omega\lambda_D^2/\mathcal{D})\tanh(\beta d/2)/(i\omega\lambda_D^2\beta)} \quad (5)$$

where S is the electrode area, $\beta^2 = i\omega/D + 1/\lambda_D^2$, with $\mathcal{E}(i\omega) = i\omega + \beta\tanh(d\beta/2)\bar{\kappa}_\alpha(i\omega)$, and $\bar{\kappa}_\alpha(i\omega) = \int_0^\infty du\int_0^1 d\bar{\nu}(i\omega)\ {}^{\bar{\nu}}\kappa_\alpha(u, \bar{\nu})e^{-i\omega u}$. $\lambda_D = \sqrt{\varepsilon k_B T/(2Nq^2)}$ is the Debye screening length. This is the impedance of model I.

Now, let us recall the final expression for the impedance of model II, worked out in ref 2. It is defined as

$$\mathcal{Z}_{\mathrm{PNPA},2} = \mathcal{R}_\infty\frac{(i\omega\tau)^\gamma + \frac{\tanh(\mathcal{M}q_a)}{\mathcal{M}q_a}}{(i\omega\tau)^\gamma(1 + (i\omega\tau)) + (i\omega\tau - (i\omega\tau)^\gamma)\frac{\tanh(\mathcal{M}q_a)}{\mathcal{M}q_a}} \quad (6)$$

where $\mathcal{R}_\infty = 1/G_\infty$, G_∞ is the high-frequency-limiting conductance, $\tau \equiv \mathcal{R}_\infty C_\infty$, C_∞ is the high-frequency-limiting bulk capacitance, $\mathcal{M} \equiv L/(2L_D)$, the number of Debye lengths in half the cell length, $q_a = (1 + (i\omega\tau)^\gamma)^{1/2}$, and $0 < \gamma \leq 1$. For $\gamma = 1$, eq 6 corresponds to the standard PNP model.[24] For the case where $\gamma < 1$, eq 6 can be considered an extension of the PNP model, which involves CPE-like behavior at low frequencies. It is also interesting to note that, in eq 6, the parameter γ is also present in q_a in contrast to the parameter β of eq 5 related to the solution of the diffusion equation. This model may also include, in its LEVM instantiation,[25] arbitrary mobilities of the two charge types and possible specific adsorption,[26] among others.[27] It is worth mentioning that this model has also been shown to fit experimental data sets of several disparate ionically and electronically conducting materials well.[12,28] In this way as well, this model is able to cover those experimental scenarios which are not suitably described in terms of the standard approaches similar to model I. In addition, this model can be further extended when judicious choices for the kernel are performed, inspired by the physical behavior of the systems being analyzed. In view of its generality and mathematical robustness, it may be considered as a fundamental framework to tackle the very rich complexity of experimental data arising from many different systems.

To investigate a connection between eq 5 (model I) and the well-established impedance given by eq 6 (model II), we first analyze these equations in the limit of low frequency and, after that, in the opposite limit. In the low-frequency limit, eq 5 can be approximated by

$$\mathcal{Z}_{\mathrm{PNPA},1} \approx \frac{\lambda^2 d}{\varepsilon SD} + \frac{2\lambda}{\varepsilon S}\frac{1}{i\omega + \bar{\kappa}_\alpha(i\omega)/\lambda} \quad (7)$$

Equation 7 contains two terms, in which one is frequency independent. This term is directly related to the bulk properties and represents a resistance of the electrolytic cell to the mobility of the ions. The second term, which depends on the frequency, is related to surface effects; i.e., it is connected to the properties of the electrode surface in contact with the sample. In this context, an important issue is to know how $\bar{\kappa}_\alpha(i\omega)$ is connected to $\mathcal{Z}$, from which the information about the surface of the electrode can be obtained, as discussed in refs 29−31. In particular, from this term, one can deduce the behavior $\mathcal{Z} \sim 1/(i\omega)^\delta$, with $0 < \delta < 1$, which has been observed in several experimental scenarios.[32−37]

On the other hand, eq 6, in the limit of low frequency, yields

$$\mathcal{Z}_{\mathrm{PNPA},2} \approx \mathcal{R}_\infty + \frac{2L_D}{L(i\omega\tau)^\gamma}\mathcal{R}_\infty \quad (8)$$

which, similarly to eq 7, may also manifest the behavior $\mathcal{Z} \sim 1/(i\omega)^\delta$ in the low-frequency limit. By performing a simple comparison between eq 7 and eq 8, we obtain that

$$\mathcal{R}_\infty = \frac{\lambda_D^2 d}{\varepsilon SD} \quad (9)$$

and

$$\bar{\kappa}_\alpha(i\omega) = \frac{D}{2\lambda_D L_D}[(i\omega\tau)^\gamma] - i\omega \quad (10)$$

Equation 9 connects the properties of resistance of the bulk present in both models, and in particular, it shows that $G_\infty \propto D$; i.e., the conductance is proportional to the diffusion coefficient of the ions. Equation 10 permits us to connect parameter γ with parameter ν present in eq 4 and, consequently, with surface effects. Equation 10 implies eq 4, with $\kappa(t, \nu) = \kappa_1\delta(t)\delta(\nu - \gamma) - \kappa_2\delta(t)\delta(\nu - 1)$, where κ_1 and κ_2 are constants.

To proceed further, we consider the high-frequency limit, i.e., $\omega \to \infty$, of both models. For eq 5, we obtain

$$\mathcal{Z}_{\mathrm{PNPA},1} \approx \frac{dD}{\epsilon\mathcal{S}\lambda_D^2\omega^2} \quad (11)$$

whereas for eq 6

$$\mathcal{Z}_{\mathrm{PNPA},2} \approx \frac{\mathcal{R}_\infty}{\tau^2\omega^2} \quad (12)$$

From the above expressions, we conclude that $\tau = \lambda_D^2/D$. These results were obtained by assuming $d = L$. The comparison performed in these limits does not permit us to connect directly the Debye length defined in eq 5 with the one proposed in eq 6.

Figure 2 illustrates eqs 5 and 6 by taking into account the connections performed in the low- and high-frequency limits for both models. We observe that one impedance formula can reproduce the other one in all limits of frequency for different values of γ.

Figure 3 considers both models to describe the experimental data obtained in the framework of the impedance spectroscopy technique for Milli-Q deionized water (see, e.g., ref 38).

The previous discussion about the models based on eqs 5 and 6 has shown that they can be related to one another, and both are able to describe experimental scenarios. Another interesting point about these models is concerned with the ionic motion within the electrolytic cell in the low-frequency limit, where the diffusion plays an important role. This point may be accessed through the electrical conductivity, which can be connected to the mean square displacement, thus giving information about the diffusion process. Following the

DOI: 10.1021/acs.jpcb.9b06263
J. Phys. Chem. B 2019, 123, 7885−7892

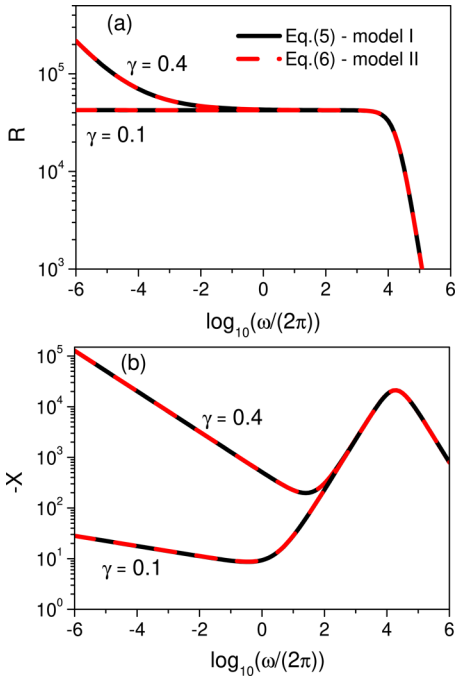

Figure 2. Behavior of real (R) and imaginary (X) parts of the impedance given by eqs 5 (model I) and 6 (model II). We consider, for simplicity, $S = 3.14 \times 10^{-4}$ m^2, $d = 10^{-3}$ m, $D = 4.7 \times 10^{-8}$ m^2 s^{-1}, $\lambda_D = 1.99 \times 10^{-7}$ m, $\kappa = 7.3 \times 10^{-3}$ ms^{-1}, and $\epsilon = 72\epsilon_0$ ($\epsilon_0 = 8.85 \times 10^{-12}$ C (V m)$^{-1}$). Note the overlap between these curves showing that for suitable conditions these models can be equivalent.

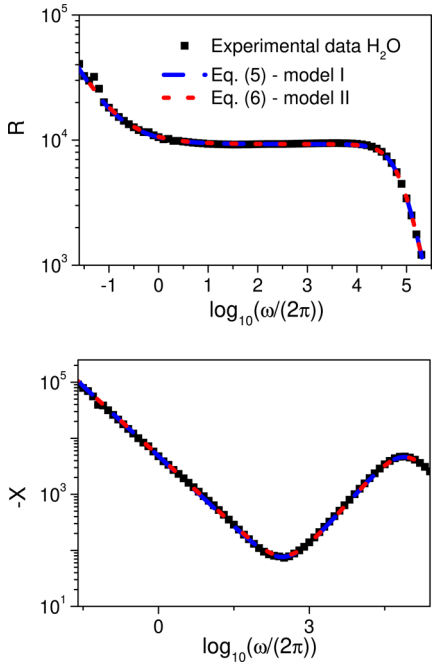

Figure 3. Behavior of real and imaginary parts of the impedance given by eqs 5 and 6. We consider, for simplicity, $S = 3.14 \times 10^{-4}$ m^2, $d = 10^{-3}$ m, $D = 3.4 \times 10^{-8}$ m^2 s^{-1}, $\lambda_D = 8.4 \times 10^{-8}$ m, $\kappa = 1.18 \times 10^{-6}$ ms^{-1}, $\epsilon = 80\epsilon_0$ ($\epsilon_0 = 8.85 \times 10^{-12}$ C(V m)$^{-1}$), and $\gamma = 0.21$.

developments performed in refs 9, 39, and 40, it is possible to relate the electrical conductivity with the mean square displacement, i.e., $\sigma(\omega) \propto D(\omega)$, and investigate the behavior of the system in the low-frequency limit. For the scenario discussed here, after some calculation, it is possible to show that the conductivity, in the low-frequency limit, can be approximated to $\sigma \approx \bar{\sigma}\omega^{\gamma}$ with $\bar{\sigma} = (\bar{\kappa}/\lambda_D)C\cos(\pi\gamma/2)$ and $C = \varepsilon S/(2\lambda_D)$, where the effect of the surface on conductivity is evident due to the presence of $\bar{\kappa}$ in $\bar{\sigma}$. By applying the procedure described in refs 39 and 40, we can show that $\langle(\Delta z)^2\rangle \propto t^{1-\gamma}$, which is a characteristic of anomalous diffusion. This result provides an important bridge between an electrical measurement and the phenomenological descriptions of ionic motion and can be also verified in other contexts.[9] Figure 4 depicts the dependence of the electrical conductivity on the frequency of the applied electric field. Both models fit the experimental curve well.

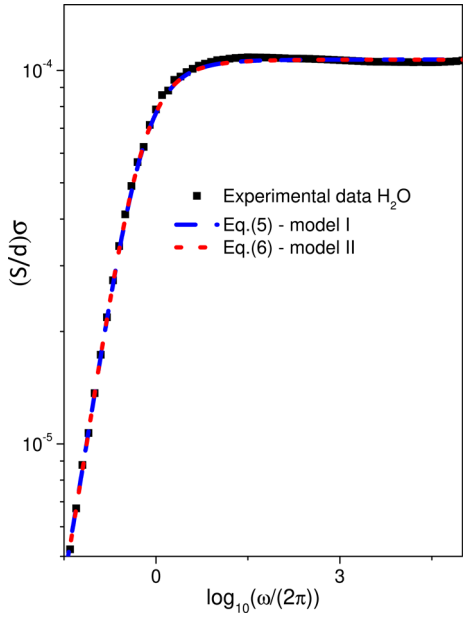

Figure 4. Comparison of the behavior of the experimental electrical conductivity data $\sigma = dR/(S|Z|^2)$ and the ones obtained from the real and imaginary parts of the impedance given by eqs 5 and 6. We consider, for simplicity, $S = 3.14 \times 10^{-4}$ m^2, $d = 10^{-3}$ m, $D = 3.4 \times 10^{-8}$ m^2 s^{-1}, $\lambda_D = 8.4 \times 10^{-8}$ m, $\kappa = 1.18 \times 10^{-6}$ ms^{-1}, $\epsilon = 80\epsilon_0$ ($\epsilon_0 = 8.85 \times 10^{-12}$ C (V m)$^{-1}$), and $\gamma = 0.21$. It shows complete agreement between the theoretical predictions and the experimental data.

BAYESIAN INVERSION

Motivation. Uncertainties between the real world and its mathematical description occur in every physical model, on one hand due to errors caused by limitations of measurement accuracy and on the other hand because of additional unavoidable inaccuracies due to the nature of the subject. Whenever a realistic situation is to be described by a model, there are certain parameters which are affected by these various uncertainties. For this reason, we consider the problem at hand in the context of probability theory.

The statistical model

$$M_i = f(t_i, Q) + \epsilon_i \tag{13}$$

is used. The function f is the mathematical description of the model. The random variable M corresponds to the measurements. Q is a random vector which denotes the parameters in our model, and t_i represents the independent variables. The values ϵ_i summarize the errors and uncertainties in each component. To use the results and methods below, there are

DOI: 10.1021/acs.jpcb.9b06263
J. Phys. Chem. B 2019, 123, 7885−7892

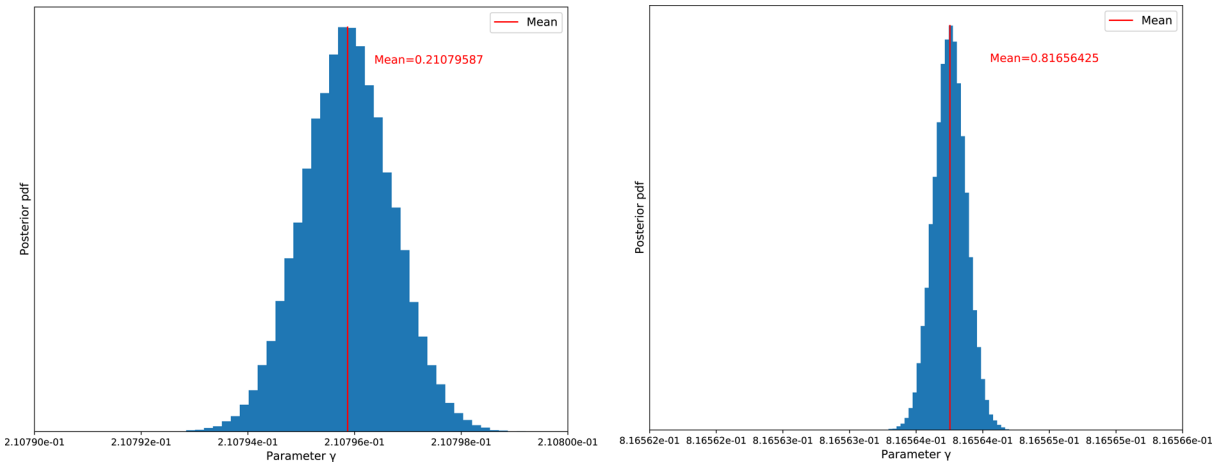

Figure 5. Marginal histograms for the parameter γ estimated from eqs 5 (left) and 6 (right) illustrating the corresponding posterior pdfs obtained by the DRAM algorithm.

some requirements to these errors: they are additive, independent, identically distributed (IID), unbiased, and mutually independent from the random variables Q.

Bayes' Theorem. We use Bayes' theorem for the inverse problem (see refs 41 and 42), and we use the version reformulated using density functions and extended with the total probability theorem.

Bayes' Theorem for Inverse Problems.[42] Let $\pi_0(q)$ be the prior probability density function for the realizations q of the random parameters Q. Let m be a realization of measurement M. Then, the posterior density of Q, given the measurements m, is

$$\pi(q|m) = \frac{\pi(m|q)\pi_0(q)}{\int_{\Omega_q} \pi(m|q)\pi_0(q)\,\mathrm{d}q} \tag{14}$$

where Ω_q is the space of parameters q.

The prior probability π_0 contains the information about the parameters Q before information has flowed through the known measurements m. The likelihood function depends on the model and is responsible for updating the posterior density with the new knowledge. It also contains information about the distribution of known errors.

Now the aim is to calculate $\pi(q)$, which denotes the distribution of the random variable Q under the conditions that the random variable M was realized by the concrete measurements m. Then, the desired parameters q can be calculated from the posterior distribution using special estimators (e.g., the mean value) including confidence intervals, etc.

Markov-Chain Monte Carlo Methods. In the implementation, the problem is that the calculation of the often high-dimensional integral in the denominator is much too expensive. This motivates the use of an alternative to calculating the integral in the denominator directly. The method we use is to construct a unique and stationary Markov chain whose stationary distribution is the same as the posteriori distribution of the unknown parameters.

Assuming an irreducible and aperiodic Markov chain, the uniqueness of the distribution can be shown. The required statistical properties are generated by the detailed balance condition for the transition probabilities within the chain. The chain can be constructed, and the necessary properties are ensured by the classic Metropolis–Hastings algorithm.

Delayed-Rejection Adaptive-Metropolis Algorithm. The method used in this work is the Delayed-Rejection Adaptive-Metropolis (DRAM) algorithm,[43] which is a modified version of the Metropolis–Hastings algorithm with better convergence properties. The modifications consist of essentially two parts: The adaptive component allows already learned information about the posterior distribution to be integrated into the running Markov chain. Delayed rejection modifies the proposal function in a specific way to increase the mixing of the chain.

DRAM Algorithm.[42,43]

1. Choose design parameters n_s, σ_s^2, k_0, and the number N_{sample} of chain iterates
2. Determine $q^0 := \text{argmin}_q \sum_{i=1}^{n}(m_i - f_i(q))^2$
3. Set $SS_q^0 := \sum_{i=1}^{n}(m_i - f_i(q^0))^2$
4. Compute initial variance estimate $s_0^2 := \frac{SS_q^0}{n-p}$
5. Construct covariance estimate $V := s_0^2(\chi^T(q^0)\chi(q^0))^{-1}$ and $R := \text{chol}(V)$
6. For $k = 1 : N_{\text{samples}}$
   (a) Sample $z_k \sim N(0, I_p)$
   (b) Construct candidate $q^* := q^{k-1} + Rz_k$
   (c) Sample $u_\alpha \sim U(0,1)$
   (d) Compute $SS_{q^*} := \sum_{i=1}^{n}(m_i - f_i(q^*)^2$
   (e) Compute $\alpha(q^*|q^{k-1}) := \min(1, e^{-(SS_{q^*} - SS_{q^{k-1}})/2s_{k-1}^2})$
   (f) If $u_\alpha < \alpha$
   Set $q^k := q^*$, $SS_{q^k} := SS_{q^*}$
   I. Set the design parameter γ_2
   II. Sample z_k $N(0, I_p)$
   III. Construct second-stage candidate $q^{*2} := q^{k-1} + \gamma_2 R_k z_k$
   IV. Sample $u_\alpha \sim U(0,1)$
   V. Compute $SS_{q^{*2}} := \sum_{i=1}^{n}(m_i - f_i(q^{*2}))^2$
   VI. Compute $\alpha_2(q^{*2}|q^{k-1}, q^*)$
   VII. If $u_\alpha < \alpha$
   Set $q^k := q^{*2}$,$SS_{q^k} := SS_{q^{*2}}$
   Set $q^k := q^{k-1}$, $SS_{q^k} := SS_{q^{k-1}}$
   (g) If $\text{mod}(k, k_0) = 1$
   Update $V_k = s_p \,\text{cov}(q^0, q^1, q^2, \ldots, q^k)$
   $V_k := V_{k-1}$
   (h) Update $R_k := \text{chol}(V_k)$

Convergence. In general, there are two questions regarding convergence: How to choose a proposal function to ensure sufficiently good mixing of the chain and how to check if the chain is long enough and reflects the desired

DOI: 10.1021/acs.jpcb.9b06263
J. Phys. Chem. B 2019, 123, 7885−7892

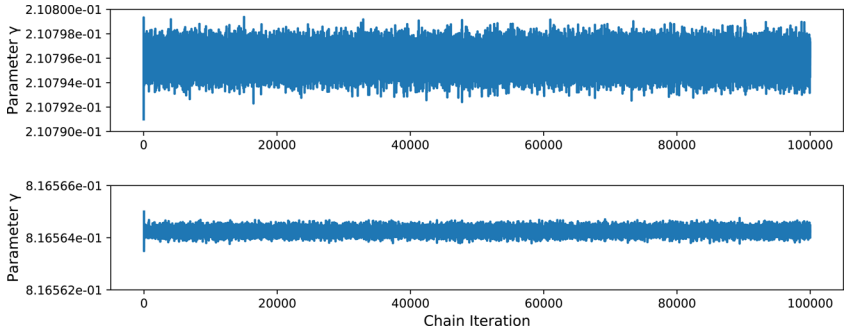

Figure 6. Sample paths for the parameter γ estimated from eqs 5 (top) and 6 (bottom) using the DRAM algorithm.

statistical properties. In contrast to the classical approach using the Metropolis–Hastings algorithm, the proposal function is calculated by the algorithm itself in case of DRAM. The remaining question can be checked by various statistical tests. The method chosen here is the calculation of the autocorrelation for subchains with length L and lag h. The autocorrelation is defined as

$$\mathrm{AC}(L, h) := \frac{\sum_{i=1}^{L-j}(q_i - \overline{q})(q_{i+h} - \overline{q})}{\sum_{i=1}^{L}(q_i - \overline{q})^2} \tag{15}$$

In the equation, the q_i are the elements of the chain and $\overline{q}$ their mean. It is a measure of how independent the samples are and how well the mixing works. Low autocorrelation implies fast convergence.

Implementation, Design Parameters, and Results. The algorithm was implemented in the programming language *Julia*[44] and the following values were selected as design parameters: We choose $s_p := 2.38$, $\gamma_2 := 0.2$, the adoption interval $k_0 := 100$, the error $\sigma_s^2 := 0.01$, and a chain length of $N_{\mathrm{Sample}} = 100\,000$.

The Bayesian estimation technique was applied to the physical model in order to extract the model parameter γ from eqs 5 and 6. In Figure 5, the marginal histograms of the parameter using the DRAM algorithm are illustrated, which show the corresponding posterior probability distributions.

Figure 6 displays trace plots of the generated Markov chains by means of DRAM algorithm showing the convergence of the chains to their true values.

The autocorrelation plots for the parameter γ are displayed in Figure 7 underlining the convergence of the MCMC method by this statistical check.

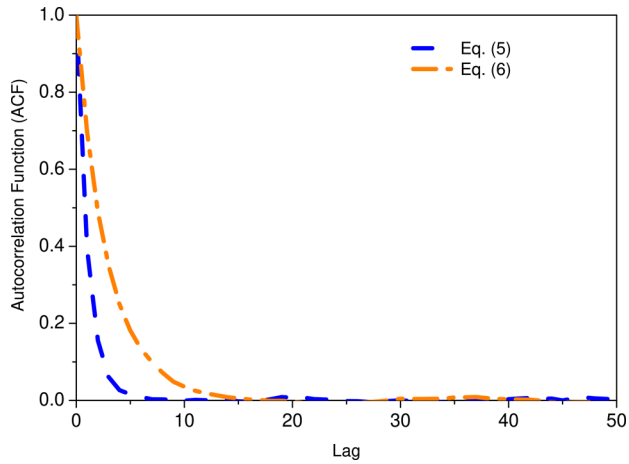

Figure 7. Autocorrelation plots for the parameter γ estimated from eqs 5 and 6 showing the convergence of the corresponding Markov chains.

CONCLUSIONS

We have analytically investigated a connection between two different extensions of the PNP model used to analyze the experimental data obtained with the technique of impedance spectroscopy. The first model (model I) is based on fractional calculus, and the second one (model II) was proposed in ref 2, but both are aimed at also incorporating anomalous diffusive behavior in their formulation. We demonstrate that these two models can be analytically related in the low-frequency limit. In addition, in this limit both models display a constant phase element behavior found in several experimental contexts, i.e., $\mathcal{Z} \sim 1/(i\omega)^{\delta}$, when an equivalent circuit description is taken into account.

We have also analytically related these two models in the limit of high frequency and, finally, analyzed their predictions for a prototypical experimental context. A very good agreement between the models and the experimental data was obtained for the impedance spectroscopy data regarding a sample of Milli-Q water. Indeed, both models are shown to be suitable to describe the experimental behavior in the whole frequency range, in contrast to the standard formulations of PNP model.

We remark that, in view of its general formulation in terms of fractional derivatives and integro-differential boundary conditions, model I can be directly extended to other situations just by choosing a different kernel in the boundary conditions. This enables it to describe different processes on the surface of the electrodes by simply adjusting the boundary conditions for the specific system being considered. In addition, we have also analyzed the behavior of electrical conductivity, which has provided evidence that the models analyzed here may be useful to better understand the ionic dynamics in different experimental scenarios.

Furthermore, we could successfully apply the Bayesian estimation method to determine the previously unknown parameter γ in the two models. The Markov chains converge very rapidly, which was confirmed by the associated autocorrelation function.

AUTHOR INFORMATION

Corresponding Author

*E-mail: rzola@utfpr.edu.br.

ORCID

L. R. Evangelista: 0000-0001-7202-1386

R. S. Zola: 0000-0003-4930-5262

DOI: 10.1021/acs.jpcb.9b06263
J. Phys. Chem. B 2019, 123, 7885−7892

Present Address

△L.R.E.: Dipartimento di Scienza Applicata del Politecnico di Torino, Corso Duca degli Abruzzi 24, 10129 Torino, Italia

Notes

The authors declare no competing financial interest.

■ ACKNOWLEDGMENTS

This work was partially supported by the National Institutes of Science and Technology of Complex Fluids—INCT-FCx (L.R.E. and R.S.Z.) and Complex Systems—INCT-SC (E.K.L.). L.T., D.P., T.S., C.H., and I.P. acknowledge the support from the bilateral research project MK 07/2018, WTZ Mazedonien S&T Macedonia 2018−20, funded under the intergovernmental Macedonian−Austrian agreement. L.T., D.P., and C.H. acknowledge support by the FWF (Austrian Science Fund) START Project Y660 PDE Models for Nanotechnology.

■ REFERENCES

(1) *Impedance Spectroscopy: Theory, Experiment and Applications*, 3rd ed.; Barsoukov, E., Macdonald, J. R., Eds.; Wiley-Interscience: New York, 2005.

(2) *Characterization of Materials*; Kaufmann, E. N., Ed.; John Wiley & Sons: New York, 2012.

(3) Barbero, G.; Evangelista, L. R. *Adsorption Phenomena and Anchoring Energy in Nematic Liquid Crystals*; CRC Press: New York, 2005.

(4) Chang, H.; Jaffe, G. Polarization in Electrolytic Solutions. Part I. Theory. *J. Chem. Phys.* **1952**, *20*, 1071−1077.

(5) Evangelista, L. R.; Lenzi, E. K. *Fractional Diffusion Equations and Anomalous Diffusion*; Cambridge University Press: United Kingdom, 2018.

(6) Jorcin, J.; Orazem, M. E.; Pébère, N.; Tribollet, B. CPE Analysis by Local Electrochemical Impedance Spectroscopy. *Electrochim. Acta* **2006**, *51*, 1473−1479.

(7) Silva, F.R.G.B.; Rossato, R.; Lenzi, E.K.; Zola, R.S.; Ribeiro, H.V.; Lenzi, M.K.; Goncalves, G. Electrolytic Cell Containing Different Groups of Ions with Anomalous Diffusion Approach. *J. Electroanal. Chem.* **2015**, *746*, 25−30.

(8) Silva, F. R. G. B.; Ribeiro, H. V.; Lenzi, M. K.; Petrucci, T.; Michels, F. S.; Lenzi, E. K. Fractional Diffusion Equations and Equivalent Circuits Applied to Ionic Solutions. *Int. J. Electrochem. Sci.* **2014**, *9*, 1892−1901.

(9) Lenzi, E. K.; Zola, R. S.; Ribeiro, H. V.; Vieira, D. S.; Ciuchi, F.; Mazzulla, A.; Scaramuzza, N.; Evangelista, L. R. Ion Motion in Electrolytic Cells: Anomalous Diffusion Evidences. *J. Phys. Chem. B* **2017**, *121*, 2882−2886.

(10) Lenzi, E. K.; Zola, R. S.; Rossato, R.; Ribeiro, H. V.; Vieira, D. S.; Evangelista, L. R. Asymptotic Behaviors of the Poisson-Nernst-Planck Model, Generalizations and Best Adjust of Experimental Data. *Electrochim. Acta* **2017**, *226*, 40−45.

(11) Ribeiro de Almeida, R. R.; Evangelista, L. R.; Lenzi, E. K.; Zola, R. S.; Jakli, A. Electrical Transport Properties and Fractional Dynamics of Twist-Bend Nematic Liquid Crystal Phase. *Commun. Nonlinear Sci.* **2019**, *70*, 248−256.

(12) Macdonald, J. R.; Evangelista, L. R.; Lenzi, E. K.; Barbero, G. Comparison of Impedance Spectroscopy Expressions and Responses of Alternate Anomalous Poisson-Nernst-Planck Diffusion Equations for Finite-Length Situations. *J. Phys. Chem. C* **2011**, *115*, 7648−7655.

(13) Ciuchi, F.; Mazzulla, A.; Scaramuzza, N.; Lenzi, E. K.; Evangelista, L. R. Fractional Diffusion Equation and the Electrical Impedance: Experimental Evidence in Liquid-Crystalline Cells. *J. Phys. Chem. C* **2012**, *116*, 8773−8777.

(14) Kumar, R.; Kant, R. Theory of Generalized Gerischer Admittance of Realistic Fractal Electrode. *J. Phys. Chem. C* **2009**, *113*, 19558−19567.

(15) Sunde, S.; Lervik, I. A.; Tsypkin, M.; Owe, L. E. Impedance Analysis of Nanostructured Iridium Oxide Electrocatalysts. *Electrochim. Acta* **2010**, *55*, 7751−7760.

(16) Batalioto, F.; Duarte, A. R.; Barbero, G.; Neto, A. M. F. Dielectric Dispersion of Water in the Frequency Range from 10 mHz to 30 MHz. *J. Phys. Chem. B* **2010**, *114*, 3467−3471.

(17) Basu, T.; Goswami, M. M.; Middya, T. R.; Tarafdar, S. Morphology and Ion-Conductivity of Gelatin $LiClO_4$ Films: Fractional Diffusion Analysis. *J. Phys. Chem. B* **2012**, *116*, 11362−11369.

(18) Santoro, P. A.; de Paula, J. L.; Lenzi, E. K.; Evangelista, L. R. Anomalous Diffusion Governed by a Fractional Diffusion Equation and the Electrical Response of an Electrolytic Cell. *J. Chem. Phys.* **2011**, *135*, 114704.

(19) Ciuchi, F.; Mazzulla, A.; Scaramuzza, N.; Lenzi, E. K.; Evangelista, L. R. Fractional Diffusion Equation and the Electrical Impedance: Experimental Evidence in Liquid-Crystalline Cells. *J. Phys. Chem. C* **2012**, *116*, 8773.

(20) Barbero, G.; Scalerandi, M. Similarities and Differences Among The Models Proposed For Real Electrodes in The Poisson-Nernst-Planck Theory. *J. Chem. Phys.* **2012**, *136*, 084705.

(21) Barbero, G. Influence of Adsorption Phenomenon on the Impedance Spectroscopy of a Cell of Liquid. *Phys. Rev. E* **2005**, *71*, 062201.

(22) Barbero, G.; Evangelista, L. R. *Adsorption Phenomena and Anchoring Energy in Nematic Liquid Crystals*; Taylor & Francis: London, 2006.

(23) Rezaei Niya, S. M. R.; Hoorfar, M. On a Possible Physical Origin of the Constant Phase Element. *Electrochim. Acta* **2016**, *188*, 98−102.

(24) Macdonald, J. R. Utility of Continuum Diffusion Models for Analyzing Mobile-Ion Immittance Data: Electrode Polarization, Bulk, and Generation-Recombination Effects. *J. Phys.: Condens. Matter* **2010**, *22*, 495101.

(25) http://jrossmacdonald.com/levmlevmw/.

(26) Macdonald, J. R.; Franceschetti, D. R. Theory of Smallsignal AC Response of Solids and Liquids with Recombining Mobile Charge. *J. Chem. Phys.* **1978**, *68*, 1614−1637.

(27) http://jrossmacdonald.com/.

(28) Macdonald, J. R. Effects of Different Boundary Conditions on the Response of Poisson-Nernst-Planck Impedance Spectroscopy Analysis Models and Comparison with a Continuous-Time Random-Walk Model. *J. Phys. Chem. A* **2011**, *115*, 13370−13380.

(29) Liu, S. H. Fractal Model for AC Response of a Rough Interface. *Phys. Rev. Lett.* **1985**, *55*, 529−532.

(30) Rammelt, U.; Reinhard, G. On the Applicability of a Constant Phase Element (CPE) to the Estimation of Roughness of Solid Metal-Electrodes. *Electrochim. Acta* **1990**, *35*, 1045−1049.

(31) Sapoval, B.; Chazalviel, J. N.; Peyriere, J. Electrical Response Of Fractal And Porous Interfaces. *Phys. Rev. A: At., Mol., Opt. Phys.* **1988**, *38*, 5867−5887.

(32) Nyikos, L.; Pajkossy, T. Fractal Dimension and Fractional Power Frequency-Dependent Impedance of Blocking Electrodes. *Electrochim. Acta* **1985**, *30*, 1533−1540.

(33) Sapoval, B. Electrodes and Constant Phase-Angle Response - Exact Examples and Counter Examples. *Solid State Ionics* **1987**, *23*, 253−259.

(34) Pajkossy, T. Electrochemistry at Fractal Surfaces. *J. Electroanal. Chem. Interfacial Electrochem.* **1991**, *300*, 1−11.

(35) Halsey, T. C.; Leibig, M. The Double-Layer Impedance at a Rough-Surface - Theoretical Results. *Ann. Phys.* **1992**, *219*, 109−147.

(36) Sapoval, B. General Formulation of Laplacian Transfer Across Irregular Surfaces. *Phys. Rev. Lett.* **1994**, *73*, 3314−3316.

(37) Grebenkov, D. S.; Filoche, M.; Sapoval, B. Mathematical Basis For a General Theory of Laplacian Transport Towards Irregular Interfaces. *Phys. Rev. E* **2006**, *73*, 021103.

(38) Lenzi, E. K.; Ribeiro, H. V.; Zola, R. S.; Evangelista, L. R. Fractional Calculus in Electrical Impedance Spectroscopy: Poisson-Nernst-Planck Model and Extensions. *Int. J. Electrochem. Sci.* **2017**, *12*, 11677−11691.

DOI: 10.1021/acs.jpcb.9b06263
J. Phys. Chem. B 2019, 123, 7885−7892

(39) Scher, H.; Lax, M. Stochastic Transport in a Disordered Solid. I. *Phys. Rev. B* **1973**, *7*, 4491−4502.
(40) Scher, H.; Lax, M. Stochastic Transport in a Disordered Solid. II. *Phys. Rev. B* **1973**, *7*, 4502−4519.
(41) Thapa, S.; Lomholt, M. A.; Krog, J.; Cherstvy, A. G.; Metzler, R. Bayesian Analysis of Single-Particle Tracking Data Using the Nested-Sampling Algorithm: Maximum-Likelihood Model Selection Applied to Stochastic-Diffusivity Data. *Phys. Chem. Chem. Phys.* **2018**, *20*, 29018−29037.
(42) Smith, R. C. *Uncertainty Quantification: Theory, Implementation, and Applications*; SIAM, 2013; Vol. *12*.
(43) Haario, H.; Laine, M.; Mira, A.; Saksman, E. Dram: Efficient Adaptive MCMC. *Statistics and Computing* **2006**, *16*, 339−354.
(44) Bezanson, J.; et al. *Julia: The Julia Programming Language, v1.0*; 2018. https://julialang.org/

DOI: 10.1021/acs.jpcb.9b06263
J. Phys. Chem. B 2019, 123, 7885−7892